nature sustainability

Brief Communication

https://doi.org/10.1038/s41893-026-01813-y

Scalable synthesis of graphitic aggregates for high-rate battery anode

Received: 1 January 2024

Accepted: 16 March 2026

Published online: 17 April 2026

Check for updates

Jiangtao Hu[1] ✉, Pei Liu[1], Shenghua Ye[1,2] ✉, Chao Peng[3] ✉, Tao Huang[1], Rui Mei[4], Xuming Yang[1], Liewu Li[1], Jishou Piao[1], Biao Jin[5], Wenwei Yu[2], Shaoluan Huang[2], Wei Xiong[2], Xiangzhong Ren[1], Ping-Heng Tan[4], Xuefeng Yu[3], Dongfeng Xue[6], Yongye Liang[7], Xiaoping Ouyang[8,9] ✉, Qianling Zhang[1] ✉ & Jianhong Liu[1,2] ✉

Graphite anodes remain the backbone of lithium-ion batteries, yet their utility is limited by sluggish lithium-ion transport kinetics under extreme conditions. Here we present a scalable method to synthesize graphitic aggregates using liquid-processable, polyacrylonitrile-based precursors, achieving a conformal graphite coating fully compatible with existing industrial workflows. This strategy effectively bypasses high-rate durability bottlenecks by tuning lithium–carbon interactions at the interface. Our findings establish liquid-processable polymer precursors as a high-throughput, manufacturable pathway towards the next generation of high-performance, sustainable energy storage.

For over three decades, graphite has remained the cornerstone of lithium-ion (Li-ion) battery anodes, sustained by its natural abundance, low cost and inherent operational safety[1–4]. Despite this dominance, its performance under extreme conditions—specifically, high-rate charging and sub-zero temperatures—presents a fundamental barrier to meeting modern energy storage demands[5–7]. These limitations are increasingly traced to sluggish Li-ion transport across the electrolyte–graphite interface, where the interplay between interfacial electronic structure and solid electrolyte interphase (SEI) formation remains tightly coupled[8–12]. While diverse strategies have emerged to engineer this interface, they frequently rely on complex, low-throughput synthesis or materials incompatible with large-scale industrial manufacturing[13–16]. Bridging this gap through scalable carbon architectures and synthesis pathways that precisely regulate graphite interfaces thus remains a critical challenge for the future of sustainable battery technologies.

Polymer-derived carbons represent a compelling, yet under-utilized, pathway towards scalable graphitic architectures. Notably, liquid-processable precursors facilitate uniform interfacial coating and batch-level processing, ensuring full compatibility with standard slurry-based electrode fabrication.

Here we report a robust synthesis involving polymerization and controlled oxidation of linear polyacrylonitrile-based molecules into ladder-type precursors, followed by high-temperature carbonization. This approach yields graphitic aggregates (GAs) characterized by a unique combination of short-range graphitic order and long-range structural disorder, synthesized in bulk under industrially relevant conditions. The fluidic nature of the precursor ensures a conformal coating on commercial graphite particles, bridging the gap between advanced materials design and established manufacturing workflows. As the interfacial electronic structure of graphite is critical to the kinetics of Li-ion transport, we employ the GA coating as an interfacial regulator

[1]Graphene Composite Research Center, College of Chemistry and Environmental Engineering, Shenzhen University, Shenzhen, People's Republic of China. [2]Shenzhen Eigen-Equation Graphene Technology Co. Ltd, Shenzhen, People's Republic of China. [3]Materials Artificial Intelligence Center, Shenzhen Institutes of Advanced Technology, Chinese Academy of Sciences, Shenzhen, People's Republic of China. [4]State Key Laboratory of Superlattices and Microstructures, Institute of Semiconductors, Chinese Academy of Sciences, Beijing, People's Republic of China. [5]Department of Chemistry, Zhejiang University, Hangzhou, People's Republic of China. [6]Shenzhen Institute for Advanced Study, University of Electronic Science and Technology of China, Shenzhen, People's Republic of China. [7]Department of Materials Science and Engineering, Southern University of Science and Technology, Shenzhen, People's Republic of China. [8]School of Materials Science and Engineering, Xiangtan University, Xiangtan, People's Republic of China. [9]Northwest Institute of Nuclear Technology, Xi'an, People's Republic of China. ✉e-mail: hujt@szu.edu.cn; yeshh@szu.edu.cn; chao.peng@siat.ac.cn; oyxp2003@aliyun.com; zhql@szu.edu.cn; liujh@szu.edu.cn

https://doi.org/10.1038/s41893-026-01813-y

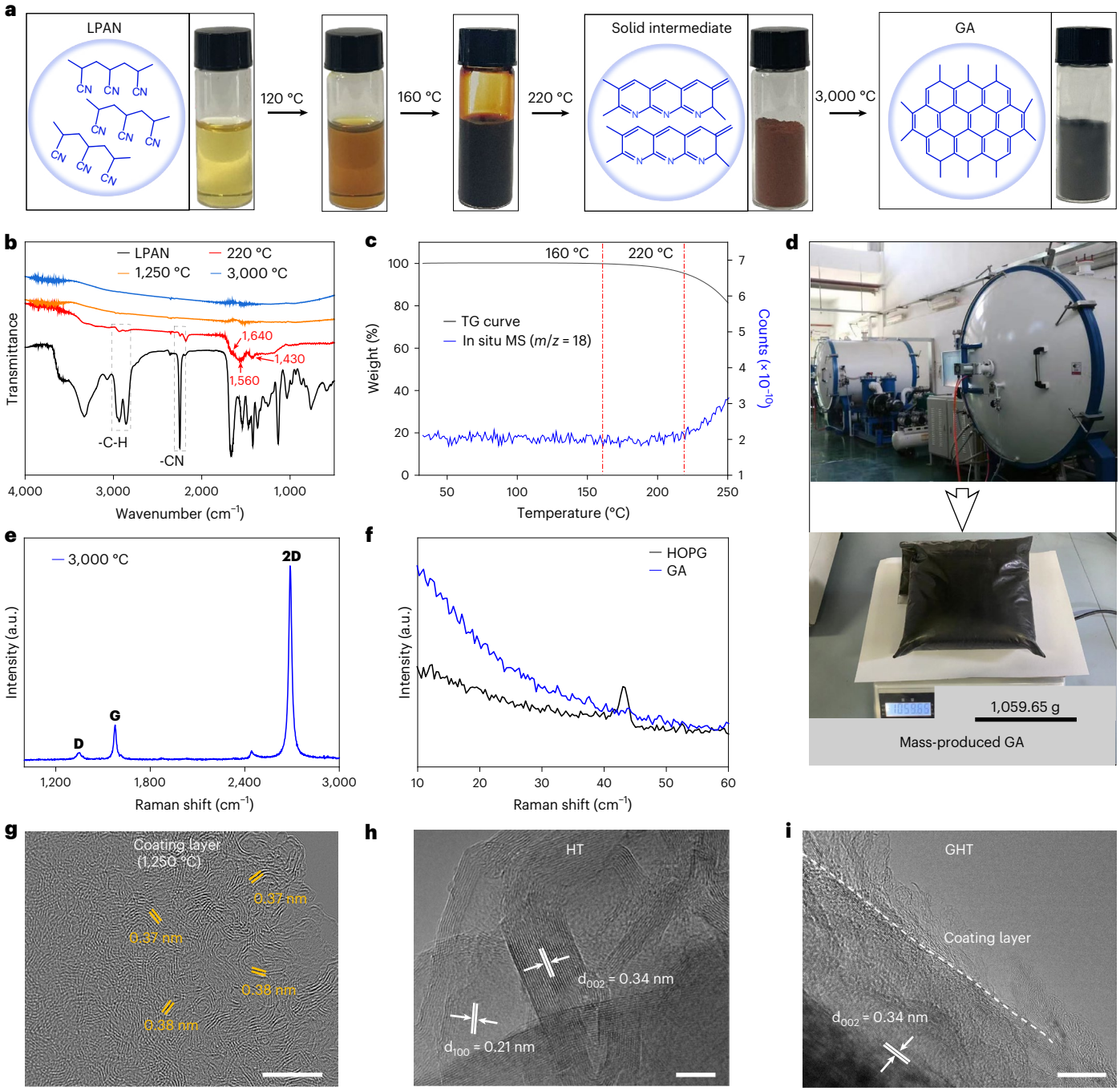

Fig. 1 | Characterizations of GA and modified anodes. a, Scalable GA synthesis route, including low-temperature pre-oxidation and high-temperature carbonization. **b**, Fourier-transform infrared spectra of LPAN, pre-oxidation at 220 °C, solid-state intermediate after calcined at 1,250 °C and the final GA calcined at 3,000 °C. **c**, Thermogravimetric and mass-spectrometric results under O_2 atmosphere, showing the thermogravimetric (TG) curve of LPAN and the mass-spectrometric (MS) signal of $m/z = 18$, which represents H_2O. **d**, Scalable GA production equipment. **e**,**f**, Raman spectra of the prepared GA under different frequencies (high frequency, **e**; low frequency, **f**). HOPG, highly oriented pyrolytic graphite. **g**, Transmission electron microscopy image of the LPAN calcined at 1,250 °C. **h**,**i**, Transmission electron microscopy images of HT (**h**) and GHT (**i**). Scale bars, 10 nm.

rather than as a conventional bulk conductive additive, enabling targeted control over lithium–carbon interactions and SEI formation. Consequently, GA-modified graphite anodes demonstrate robust high-rate durability in practical formats, retaining 87.9% capacity after 1,000 cycles at 1 C and 83.9% after 500 cycles at 3 C within 18650-type cylindrical cells, all while maintaining superior low-temperature performance.

A sustainable, scalable and cost-effective strategy—termed the linear–ladder–planar method—was developed to produce GA. As illustrated in Fig. 1a, the liquid polyacrylonitrile (LPAN) with linear structure first underwent cyclization to form a solid intermediate at 220 °C. Fourier-transform infrared spectroscopy (Fig. 1b) shows the near-complete disappearance of absorption bands for nitrile groups and carbon–hydrogen vibrations, while three new bands emerge at 1,640, 1,560 and 1,430 cm^{-1}, corresponding to a conjugated aromatic framework. Thermogravimetric and mass-spectrometric analysis (Fig. 1c) revealed minimal weight loss below 160 °C, along with a distinct colour change in LPAN, implying that a condensation reaction occurred. For LPAN, where cyano groups are the only unsaturated

functional groups, it can be inferred that the condensation of cyano groups forms hexatomic rings. A slight weight loss of between 160 °C and 220 °C, together with an increased water signal ($m/z = 18$), demonstrates that cyano group condensation is followed by dehydrogenation. Dehydrogenation of the six-membered ring structure gives rise to a conjugated structure, thereby facilitating the formation of a fused ring system (ladder structure in Fig. 1a). The red solid intermediate shown in Fig. 1a was gradually heated up to 3,000 °C under an inert atmosphere to enhance graphitization, producing a thermodynamically stable planar structure. The method achieves a production capacity of ~20 kg per batch (Fig. 1d). Raman spectroscopy of the 3,000 °C product (Fig. 1e) shows the strongest 2D peak to date[17], with minimal D-band intensity and low oxygen content (Supplementary Fig. 1), indicating a high degree of graphitization, extensive sp^2 plane and few defects. Low-frequency Raman spectroscopy of highly oriented pyrolytic graphite reveals a characteristic shear mode at 43.4 cm^{-1} (Fig. 1f). By contrast, our sample exhibits only a near-zero wavenumber inelastic scattering signal, attributed to low-energy excitations or free carriers. This observation aligns with the low-frequency Raman spectra under cross-polarization conditions (Supplementary Fig. 2), indicating the absence of the shear mode in our sample, which originates from a weak sp^2 interlayer interaction. As expected, the transmission electron microscopy images and X-ray diffraction pattern provided in Supplementary Figs. 3 and 4 reveal a graphite-like structure with an expanded interlayer spacing greater than the typical 0.34 nm, which is likely due to weak interlayer interaction. Based on these observations, the sample is identified as GAs. Moreover, the weak interlayer interaction in GAs allows for easy exfoliation into fewer layers of graphene sheets—typically fewer than five layers—using liquid nitrogen and ethyl alcohol, as shown in Supplementary Fig. 5. A gate-to-gate life cycle assessment demonstrated that our linear–ladder–planar pathway, when powered by renewable energy sources, maintains a low ecological footprint (Supplementary Fig. 6 and Supplementary Tables 1 and 2).

Beyond calcining the solid intermediate at 3,000 °C to form low-defect, highly crystalline GA, we also observed the emergence of short-range-ordered GA at 1,250 °C. These aggregates exhibited early-stage graphitization (Supplementary Figs. 7 and 8) and weak interlayer interactions with expanded interlayer spacing (Fig. 1g). Leveraging the unique architecture of short-range-ordered GA and the processability of the LPAN precursor, we modified the graphite anode via the linear–ladder–planar method by blending commercial graphite (high-temperature needle coke, named as HT) with LPAN, followed by pre-oxidation at 220 °C and graphitization at 1,250 °C, yielding a GA-modified HT material named GHT. GHT maintained morphological features like HT, but with a reduced active surface area (Supplementary Fig. 9). Transmission electron microscopy images in Fig. 1h and Supplementary Fig. 10 revealed lattice spacings of 0.34 nm and 0.21 nm for HT, corresponding to the (002) and (100) planes of graphite[18], respectively. In contrast, GHT displayed a uniform coating structure (Fig. 1i and Supplementary Fig. 11) that maintained electron conductivity (Supplementary Fig. 12).

The electrochemical performance of GHT was first evaluated in coin cells. As shown in Supplementary Fig. 13a, GHT delivers a higher initial charge capacity (350.7 mAh g^{-1}) and Coulombic efficiency (96.27%) compared to HT (337.4 mAh g^{-1} and 93.54%). GHT also displays smaller polarization in its delithiation and lithiation peaks (Supplementary Fig. 13b) and improved cycling stability, retaining 91.71% of its capacity after 200 cycles versus 79.52% for HT (Supplementary Fig. 13c). Voltage profiles further confirm that GHT-based cells maintain both capacity and working voltage during long-term cycling (Supplementary Fig. 13d). Supplementary Fig. 14 depicts that lithium deposition was not observed on the GHT surface, while serious lithium deposition was observed on HT. Rate capability was assessed using two protocols after formation cycling at 0.1 C. Under constant-charge conditions, the GHT-based cell exhibited higher capacities at all rates, whereas the HT-based cell showed rapid capacity decay above 1 C (Supplementary Fig. 13e). At 5 C, the GHT-based cell retained 76.22% of its 0.1 C capacity, notably surpassing the HT cell's 47.45% capacity. With varying charge rates and a constant discharge rate, the GHT-based cell again demonstrated superior rate performance (Supplementary Fig. 13f). These results indicate faster Li^+ intercalation kinetics for GHT, which helps explain its superior cycling stability. Post-cycling analysis reveals a uniform, stable SEI layer on GHT and suppressed lithium deposition, in contrast to the non-uniform SEI and severe decomposition on HT (Supplementary Fig. 15a–c). Electrochemical impedance spectroscopy confirms faster charge-transfer kinetics at the GHT interface (Supplementary Fig. 15d–g). These improvements are attributed to the GA's coating, which enhances interfacial ion transport and structural stability.

Building on GHT's advantages, we assembled and tested 18,650 cylindrical cells (the results are depicted in Supplementary Figs. 16–18). After 1,000 cycles, the GHT|| $LiNi_{0.5}Mn_{0.3}Co_{0.2}O_2$. cell retained 87.9% of its initial capacity, and even at a 3 C discharge rate, it maintained 83.9%. The cell also showed excellent low-temperature performance, with capacity retentions of 93.2% at 2 C and 92.2% at 3 C when tested at −10 °C. These results highlight the superior cycle life, high-rate capability and low-temperature performance of GHT||$LiNi_{0.5}Mn_{0.3}Co_{0.2}O_2$ cells.

Density functional theory (DFT) calculations were conducted to clarify the enhanced electrochemical performance of GA-coated graphite anodes (Fig. 2). As shown in Fig. 2a, pristine graphite exposes armchair and zigzag edges where SEI preferentially forms[19], and Li-ion exhibits stronger binding at edge sites than in the bulk. Li-ion binding energies are −0.48 eV at the armchair edge and −0.62 eV at the zigzag edge, both much higher than the bulk value (−0.34 eV). The strong binding at the zigzag edge originates from topological surface states associated with carbon p_z orbitals, which stabilize Li-ion and extend partially into the bulk. After GA coating, the surface effect is largely weakened. In the armchair-edged GA and zigzag-edged GA heterostructures (Fig. 2b), Li-ion adsorption at the GA sites is relatively weak (−0.20 to −0.24 eV), and the binding energies that occur at the heterostructures (−0.43 to −0.46 eV) are lower than those at the pristine edges (Fig. 2c). Notably, the absence of spin-polarized surface states at the zigzag-edged GA heterostructures reduces Li-ion binding by ~0.16 eV compared with pristine zigzag edges (Fig. 2d). Fig. 2e,f illustrates the crystal orbital Hamilton population of Li-ion binding at the zigzag-edged GA and zigzag edge. There is less covalent bonding below the Fermi level at around −8 eV from the Li–C σ bond, and a greater contribution of the anti-bonding component above the Fermi level at ~4 eV for zigzag-edged GA heterostructures, indicating a more ionic bonding nature of Li-ion in the zigzag/GA heterostructure by reducing the surface-state interactions, which was also verified by the local density of states and electron locational function (Supplementary Figs. 20 and 21).

The weakened surface effect leads to a shallower potential well and improved Li-ion mobility. Ab initio molecular dynamics simulations show that Li-ion diffusion is confined near pristine zigzag edges (indicated by the red regions in Fig. 2a,b), but becomes much more delocalized in zigzag-edged GA heterostructures for Li-ion mobility. Markov Chain modelling[20] reveals that Li-ion diffusion in both armchair-edged and zigzag-edged GA is about three times faster than in pristine graphite edges (1.0 μs versus 0.35 μs), as depicted in Fig. 2g,h. This indicates that GA coating effectively suppresses edge effects, facilitates rapid Li-ion transfer from the interface into the graphite bulk, and thereby enhances ion intercalation kinetics and rate performance.

In summary, we demonstrate a scalable, industrially compatible synthesis utilizing LPAN precursors to engineer unique GAs. This approach enables the formation of conformal, interfacial coatings that fundamentally alter the surface topology of graphite anodes. Our findings establish a manufacturable strategy for the next generation of high-rate, long-life energy storage systems.

https://doi.org/10.1038/s41893-026-01813-y

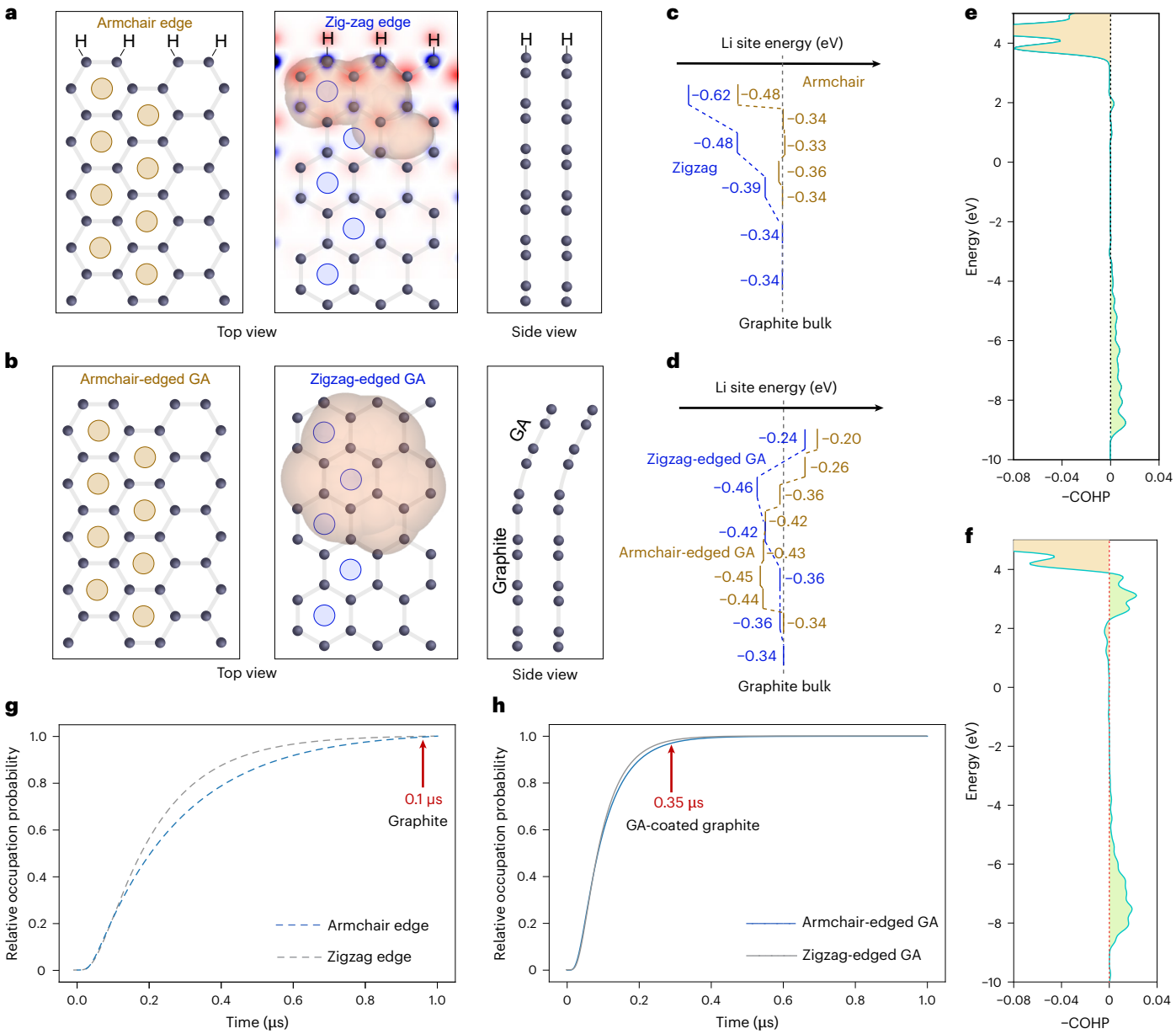

Fig. 2 | DFT calculations. a, Structures of armchair-edged and zigzag-edged graphite. **b**, GA-coated armchair and zigzag heterostructures. The red area shows the region of Li-ion mobility in molecular dynamics simulations. **c**,**d**, Energy profiles of Li-ion adsorption at different sites in **a** (**c**) and **b** (**d**). **e**,**f**, Crystal orbital Hamilton population (COHP) of Li binding at the interface site in zigzag-edged GA heterostructure (**e**) and the zigzag edge (**f**). **g**,**h**, Relative site occupation probability for Li-ion to reach a site about 19 Å distance from the initial adsorption site after being introduced at time zero at the initial adsorption site, including graphite (**g**) and GA-coated graphite (**h**).

Methods

GAs were synthesized from a LPAN precursor supplied by Shenzhen Eigen-Equation Graphene Technology Co. Ltd. The LPAN was first heated in air at 220 °C for 3 hours, turning from light yellow to dull red, and then solidifying. The resulting solid was ball-milled and then sintered at 3,000 °C for 8 hours under argon to yield a black powder. To prepare a surface-modified graphite anode, commercial graphite (HT, from the same supplier) was mixed with deionized water (1:1) and 7% LPAN under stirring for 4 hours, followed by spray drying at 180 °C. The mixture was calcined at 220 °C for 3 hours and sintered at 1,250 °C for 5 hours under nitrogen. The final product was labelled as GHT.

Reporting summary

Further information on research design is available in the Nature Portfolio Reporting Summary linked to this article.

Data availability

All the relevant data are included in the paper and the corresponding Supplementary Information. Source data are provided with this paper.

References

1. Zhu, J., Yang, D., Yin, Z., Yan, Q. & Zhang, H. Graphene and graphene-based materials for energy storage applications. *Small* **10**, 3480–3498 (2014).
2. Manthiram, A. A reflection on lithium-ion battery cathode chemistry. *Nat. Commun.* **11**, 1550 (2020).
3. Zhang, H., Yang, Y., Ren, D., Wang, L. & He, X. Graphite as anode materials: fundamental mechanism, recent progress and advances. *Energy Storage Mater.* **36**, 147–170 (2021).
4. Zhao, L. et al. Revisiting the roles of natural graphite in ongoing lithium-ion batteries. *Adv. Mater.* **34**, 2106704 (2022).

5. Cai, W. et al. A review on energy chemistry of fast-charging anodes. *Chem. Soc. Rev.* **49**, 3806–3833 (2020).
6. Jow, T. R., Delp, S. A., Allen, J. L., Jones, J.-P. & Smart, M. C. Factors limiting Li^+ charge transfer kinetics in Li-ion batteries. *J. Electrochem. Soc.* **165**, A361 (2018).
7. Yang, X.-G. et al. Asymmetric temperature modulation for extreme fast charging of lithium-ion batteries. *Joule* **3**, 3002–3019 (2019).
8. Ruggeri, I., Martin, J., Wohlfahrt-Mehrens, M. & Mancini, M. Interfacial kinetics and low-temperature behavior of spheroidized natural graphite particles as anode for Li-ion batteries. *J. Solid State Electr.* **26**, 73–83 (2022).
9. Wang, A., Kadam, S., Li, H., Shi, S. & Qi, Y. Review on modeling of the anode solid electrolyte interphase (SEI) for lithium-ion batteries. *NPJ Comput. Mater.* **4**, 15 (2018).
10. Baek, M., Kim, J., Jin, J. & Choi, J. W. Photochemically driven solid electrolyte interphase for extremely fast-charging lithium-ion batteries. *Nat. Commun.* **12**, 6807 (2021).
11. Adenusi, H., Chass, G. A., Passerini, S., Tian, K. V. & Chen, G. Lithium batteries and the solid electrolyte interphase (SEI)—progress and outlook. *Adv. Energy Mater.* **13**, 2203307 (2023).
12. Kulathuvayal, A. S. & Su, Y. Ionic transport through the solid electrolyte interphase in lithium-ion batteries: a review from first-principles perspectives. *ACS Appl. Energy Mater.* **6**, 5628–5645 (2023).
13. Jones, J.-P., Smart, M. C., Krause, F. C., Ratnakumar, B. V. & Brandon, E. J. The effect of electrolyte composition on lithium plating during low temperature charging of Li-ion cells. *ECS Trans.* https://doi.org/10.1149/07521.0001ecst (2017).
14. Abe, T., Fukuda, H., Iriyama, Y. & Ogumi, Z. Solvated Li-ion transfer at interface between graphite and electrolyte. *J. Electrochem. Soc.* **151**, A1120 (2004).
15. Fitzhugh, W. & Li, X. Modulation of ionic current limitations by doping graphite anodes. *J. Electrochem. Soc.* **165**, A2233 (2018).
16. Billaud, J., Bouville, F., Magrini, T., Villevieille, C. & Studart, A. R. Magnetically aligned graphite electrodes for high-rate performance Li-ion batteries. *Nat. Energy* **1**, 16097 (2016).
17. Li, X. et al. Large-area synthesis of high-quality and uniform graphene films on copper foils. *Science* **324**, 1312–1314 (2009).
18. Chaliyawala, H. A., Rajaram, N., Patel, R., Ray, A. & Mukhopadhyay, I. Controlled island formation of large-area graphene sheets by atmospheric chemical vapor deposition: role of natural camphor. *ACS Omega* **4**, 8758–8766 (2019).
19. Zhang, Z. et al. Operando electrochemical atomic force microscopy of solid–electrolyte interphase formation on graphite anodes: the evolution of SEI morphology and mechanical properties. *ACS Appl. Mater. Interfaces* **12**, 35132–35141 (2020).
20. Peng, C., Mercer, M. P., Skylaris, C.-K. & Kramer, D. Lithium intercalation edge effects and doping implications for graphite anodes. *J. Mater. Chem. A* **8**, 7947–7955 (2020).

Acknowledgements

We are grateful for the financial support provided by the National Natural Science Foundation of China (nos. 52202269 and 52203303), the Shenzhen Natural Science Foundation (no. 20220810155330003), the Shenzhen Science and Technology Program (CJGJZD20210408092801005), Shenzhen Key Projects of Technological Research (no. JSGG20200925145800001) and the Department of Education of Guangdong Province (no. 2022ZDZX3018).

Author contributions

J.H. and J.L. conceived the idea for this project. J.H., X.O., Q.Z. and J.L. designed the experiments and tested the physical and electrochemical properties. C.P., D.X. and X. Yu (Chinese Academy of Sciences) conducted the DFT calculations. P.-H.T. and R.M. collected the low-frequency Raman data. X. Yang (Shenzhen University), S.H., W.Y. and W.X. prepared the electrode materials and performed some of the electrochemical properties. P.L., T.H., X. Yang (Shenzhen University), L.L., S.Y., J.P., B.J., X.R. and Y.L. discussed the results and analysed the data. J.H. and S.Y. wrote and revised the paper.

Competing interests

The authors declare no competing interests.

Additional information

Supplementary information The online version contains supplementary material available at https://doi.org/10.1038/s41893-026-01813-y.

Correspondence and requests for materials should be addressed to Jiangtao Hu, Shenghua Ye, Chao Peng, Xiaoping Ouyang, Qianling Zhang or Jianhong Liu.

Peer review information *Nature Sustainability* thanks Yingying Zhang and the other, anonymous, reviewer(s) for their contribution to the peer review of this work.

nature portfolio

Corresponding author(s): Jianhong Liu

Last updated by author(s): Mar 7, 2026

Reporting Summary

Nature Portfolio wishes to improve the reproducibility of the work that we publish. This form provides structure for consistency and transparency in reporting. For further information on Nature Portfolio policies, see our Editorial Policies and the Editorial Policy Checklist.

Statistics

For all statistical analyses, confirm that the following items are present in the figure legend, table legend, main text, or Methods section.

n/a	Confirmed	
☐	☒	The exact sample size (*n*) for each experimental group/condition, given as a discrete number and unit of measurement
☐	☒	A statement on whether measurements were taken from distinct samples or whether the same sample was measured repeatedly
☒	☐	The statistical test(s) used AND whether they are one- or two-sided *Only common tests should be described solely by name; describe more complex techniques in the Methods section.*
☒	☐	A description of all covariates tested
☒	☐	A description of any assumptions or corrections, such as tests of normality and adjustment for multiple comparisons
☐	☒	A full description of the statistical parameters including central tendency (e.g. means) or other basic estimates (e.g. regression coefficient) AND variation (e.g. standard deviation) or associated estimates of uncertainty (e.g. confidence intervals)
☒	☐	For null hypothesis testing, the test statistic (e.g. *F*, *t*, *r*) with confidence intervals, effect sizes, degrees of freedom and *P* value noted *Give P values as exact values whenever suitable.*
☒	☐	For Bayesian analysis, information on the choice of priors and Markov chain Monte Carlo settings
☒	☐	For hierarchical and complex designs, identification of the appropriate level for tests and full reporting of outcomes
☒	☐	Estimates of effect sizes (e.g. Cohen's *d*, Pearson's *r*), indicating how they were calculated

Our web collection on statistics for biologists contains articles on many of the points above.

Software and code

Policy information about availability of computer code

Data collection	The morphologies of the prepared materials and the cycled electrodes were detected by scanning electron microscope (SEM, JSM 7800F, JEOL). Transmission electron microscopy (TEM, JEOL JEM-F200) were applied to characterize the material structure and SEI layer thickness. Other high resolution TEM images were performed on FEI Talos F200X with different voltages. Aberration-corrected STEM (FEI Titan Cubed Themis G2 300) at the Electron Microscopy Center of Shenzhen University was applied to observe the graphitization of the resulting samples. The graphitic aggregates quality was detected by Raman spectra (Renishaw inVia Raman microscope). The low-frequency Raman spectra were acquired using a microconfocal Raman system (Jobin-Yvon HR800). The objective lens employed had a resolution of 100x (0.9NA) and the excitation energy of the He-Ne laser is 1.96 eV. The experiment adopts 1800 gr/mm holographic grating to ensure high spectral resolution (~0.35 cm-1). The electronic conductivity comparison between the pristine graphite and the coated sample was performed by 4-Point probes measurement system, and the corresponding pressure is 1.26 kN. The surface area of the prepared samples were measured by Multi-point Method (BSD-PS). The SEI compositions were determined by X-ray photoelectron spectroscopy (XPS, Thermo Fisher Scientific) and fitted by Advantage. The binding energy were calibrated according to the C 1s peak at 284.4 eV. Nitrogen absorption–desorption isotherms were evaluated on a BESTCN 3H-2000PS2 instrument, and the specific surface areas were calculated by the multi-point BET equation. TG-MS was determined by a Netzsch STA449 F3 +Quadrupole Mass Spectrometry (QMS403D). FT-IR spectra was recorded by IR Affinity®-1 spectrometer (Shimadzu, Düsseldorf, Germany). Total electron yield (TEY) soft x ray absorption spectrum were measured at the 4B9B beamline in Beijing Synchrotron Radiation Facility (BSRF). The base pressure of the analysis chamber was better than 3 × 10−10 Torr. The photon energy was calibrated by Au 4f core level XPS of clean polycrystalline gold foil which is electrically connected to the sample.
Data analysis	Powerpoint and origin were used to conduct the data analysis.

For manuscripts utilizing custom algorithms or software that are central to the research but not yet described in published literature, software must be made available to editors and reviewers. We strongly encourage code deposition in a community repository (e.g. GitHub). See the Nature Portfolio guidelines for submitting code & software for further information.

Data

Policy information about availability of data

All manuscripts must include a data availability statement. This statement should provide the following information, where applicable:

- Accession codes, unique identifiers, or web links for publicly available datasets
- A description of any restrictions on data availability
- For clinical datasets or third party data, please ensure that the statement adheres to our policy

The data that support the findings of this study are available within the text including the Methods, and Supplemental information. Raw datasets related to the current work are available from the corresponding author on reasonable request.

Human research participants

Policy information about studies involving human research participants and Sex and Gender in Research.

Reporting on sex and gender	There are no sex- and gender-related data in our research.
Population characteristics	There are no data about the population characteristics of the human research participants in our research.
Recruitment	There are no data involving the human research participants in our research.
Ethics oversight	There are no data involving the human research participants in our research.

Note that full information on the approval of the study protocol must also be provided in the manuscript.

Field-specific reporting

Please select the one below that is the best fit for your research. If you are not sure, read the appropriate sections before making your selection.

☐ Life sciences ☐ Behavioural & social sciences ☒ Ecological, evolutionary & environmental sciences

For a reference copy of the document with all sections, see nature.com/documents/nr-reporting-summary-flat.pdf

Ecological, evolutionary & environmental sciences study design

All studies must disclose on these points even when the disclosure is negative.

Study description	Scalable synthesis of graphitic aggregates for high-rate battery anode
Research sample	Graphitic aggregates, high-rate anode
Sampling strategy	Liquid polyacrylonitrile (LPAN) is the precursor of the graphitic aggregates. During heat to 220℃ in air, LPAN was firstly pre-oxidized and trapezoidal, which experienced a distinct color changes from light yellow to dark black, and concentration changes from dilute to concentrated solution. Then, the dark product was heated at 220℃ for 3h to realize full peroxidation and molecular planarization, and the corresponding color of the product is dull red. Before calcination at 3000℃, the dull red product needs a ball milling operation. To the end, we obtained a black powder after sintering at 3000℃ for 8h under Ar atmosphere, which is proved to be the graphitic aggregates. The whole synthesis process goes through the cyclization and planarization processes from the organic linear molecules. The above graphitic aggregates synthesis route was applied to produce surface modified graphite anode. Commercial graphite (Labeled as HT, received from Shenzhen Eigen-Equation Graphene Technology Co., Ltd.) was stirred with deionized water (1:1) and 7% LPAN precursor for 4h before spray dried at 180°C. The obtained mixture was calcinated at 220°C for 3h and then sintered at 1250°C for 5h under N2 atmosphere. The final product is named as GHT. This technology is well established and is being used to produce tonnage-scale GHT anode material.
Data collection	Sample characterization were conducted on scanning electron microscope (SEM, JSM 7800F, JEOL), transmission electron microscopy (TEM，JEOL JEM-F200), Raman spectra (Renishaw inVia Raman microscope), microconfocal Raman system (Jobin-Yvon HR800), 4-Point probes measurement system, X-ray photoelectron spectroscopy (XPS, Thermo Fisher Scientific), BESTCN 3H-2000PS2 instrument, Vienna Ab initio Simulation Package (VASP), ab-initio molecular dynamics (AIMD) simulation.
Timing and spatial scale	Dec. 2021-Dec.2024
Data exclusions	No data were excluded.
Reproducibility	All attempts to repeat the experiment were successful.

Randomization	Not applicable.
Blinding	Not applicable.

Did the study involve field work? ☐ Yes ☒ No

Reporting for specific materials, systems and methods

We require information from authors about some types of materials, experimental systems and methods used in many studies. Here, indicate whether each material, system or method listed is relevant to your study. If you are not sure if a list item applies to your research, read the appropriate section before selecting a response.

Materials & experimental systems

n/a	Involved in the study
☒	☐ Antibodies
☒	☐ Eukaryotic cell lines
☒	☐ Palaeontology and archaeology
☒	☐ Animals and other organisms
☒	☐ Clinical data
☒	☐ Dual use research of concern

Methods

n/a	Involved in the study
☒	☐ ChIP-seq
☒	☐ Flow cytometry
☒	☐ MRI-based neuroimaging